Study of electromagnetic Dalitz decays $\chi_{cJ} \to \mu^+\mu^- J/\psi$

M. Ablikim,[1] M. N. Achasov,[10,d] S. Ahmed,[15] M. Albrecht,[4] M. Alekseev,[55a,55c] A. Amoroso,[55a,55c] F. F. An,[1] Q. An,[52,42] Y. Bai,[41] O. Bakina,[27] R. Baldini Ferroli,[23a] Y. Ban,[35] K. Begzsuren,[25] D. W. Bennett,[22] J. V. Bennett,[5] N. Berger,[26] M. Bertani,[23a] D. Bettoni,[24a] F. Bianchi,[55a,55c] J. Bloms,[50] I. Boyko,[27] R. A. Briere,[5] H. Cai,[57] X. Cai,[1,42] A. Calcaterra,[23a] G. F. Cao,[1,46] S. A. Cetin,[45b] J. Chai,[55c] J. F. Chang,[1,42] W. L. Chang,[1,46] G. Chelkov,[27,b,c] G. Chen,[1] H. S. Chen,[1,46] J. C. Chen,[1] M. L. Chen,[1,42] S. J. Chen,[33] Y. B. Chen,[1,42] W. Cheng,[55c] G. Cibinetto,[24a] F. Cossio,[55c] H. L. Dai,[1,42] J. P. Dai,[37,h] A. Dbeyssi,[15] D. Dedovich,[27] Z. Y. Deng,[1] A. Denig,[26] I. Denysenko,[27] M. Destefanis,[55a,55c] F. De Mori,[55a,55c] Y. Ding,[31] C. Dong,[34] J. Dong,[1,42] L. Y. Dong,[1,46] M. Y. Dong,[1,42,46] Z. L. Dou,[33] S. X. Du,[60] J. Z. Fan,[44] J. Fang,[1,42] S. S. Fang,[1,46] Y. Fang,[1] R. Farinelli,[24a,24b] L. Fava,[55b,55c] F. Feldbauer,[4] G. Felici,[23a] C. Q. Feng,[52,42] M. Fritsch,[4] C. D. Fu,[1] Y. Fu,[1] Q. Gao,[1] X. L. Gao,[52,42] Y. Gao,[44] Y. G. Gao,[6] Z. Gao,[52,42] B. Garillon,[26] I. Garzia,[24a] A. Gilman,[49] K. Goetzen,[11] L. Gong,[34] W. X. Gong,[1,42] W. Gradl,[26] M. Greco,[55a,55c] L. M. Gu,[33] M. H. Gu,[1,42] Y. T. Gu,[13] A. Q. Guo,[1] L. B. Guo,[32] R. P. Guo,[1,46] Y. P. Guo,[26] A. Guskov,[27] S. Han,[57] X. Q. Hao,[16] F. A. Harris,[47] K. L. He,[1,46] F. H. Heinsius,[4] T. Held,[4] Y. K. Heng,[1,42,46] Z. L. Hou,[1] H. M. Hu,[1,46] J. F. Hu,[37,h] T. Hu,[1,42,46] Y. Hu,[1] G. S. Huang,[52,42] J. S. Huang,[16] X. T. Huang,[36] X. Z. Huang,[33] Z. L. Huang,[31] T. Hussain,[54] N. Hsken,[50] W. Ikegami Andersson,[56] W. Imoehl,[22] M. Irshad,[52,42] Q. Ji,[1] Q. P. Ji,[16] X. B. Ji,[1,46] X. L. Ji,[1,42] H. L. Jiang,[36] X. S. Jiang,[1,42,46] X. Y. Jiang,[34] J. B. Jiao,[36] Z. Jiao,[18] D. P. Jin,[1,42,46] S. Jin,[33] Y. Jin,[48] T. Johansson,[56] N. Kalantar-Nayestanaki,[29] X. S. Kang,[34] M. Kavatsyuk,[29] B. C. Ke,[1] I. K. Keshk,[4] T. Khan,[52,42] A. Khoukaz,[50] P. Kiese,[26] R. Kiuchi,[1] R. Kliemt,[11] L. Koch,[28] O. B. Kolcu,[45b,f] B. Kopf,[4] M. Kuemmel,[4] M. Kuessner,[4] A. Kupsc,[56] M. Kurth,[1] W. Kühn,[28] J. S. Lange,[28] P. Larin,[15] L. Lavezzi,[55c] H. Leithoff,[26] C. Li,[56] Cheng Li,[52,42] D. M. Li,[60] F. Li,[1,42] F. Y. Li,[35] G. Li,[1] H. B. Li,[1,46] H. J. Li,[9,j] J. C. Li,[1] J. W. Li,[40] Ke Li,[1] L. K. Li,[1] Lei Li,[3] P. L. Li,[52,42] P. R. Li,[30] Q. Y. Li,[36] W. D. Li,[1,46] W. G. Li,[1] X. L. Li,[36] X. N. Li,[1,42] X. Q. Li,[34] X. H. Li,[52,42] Z. B. Li,[43] H. Liang,[52,42] Y. F. Liang,[39] Y. T. Liang,[28] G. R. Liao,[12] L. Z. Liao,[1,46] J. Libby,[21] C. X. Lin,[43] D. X. Lin,[15] B. Liu,[37,h] B. J. Liu,[1] C. X. Liu,[1] D. Liu,[52,42] D. Y. Liu,[37,h] F. H. Liu,[38] Fang Liu,[1] Feng Liu,[6] H. B. Liu,[13] H. L. Liu,[41] H. M. Liu,[1,46] Huanhuan Liu,[1] Huihui Liu,[17] J. B. Liu,[52,42] J. Y. Liu,[1,46] K. Y. Liu,[31] Ke Liu,[6] Q. Liu,[46] S. B. Liu,[52,42] X. Liu,[30] Y. B. Liu,[34] Z. A. Liu,[1,42,46] Zhiqing Liu,[26] Y. F. Long,[35] X. C. Lou,[1,42,46] H. J. Lu,[18] J. D. Lu,[1,46] J. G. Lu,[1,42] Y. Lu,[1] Y. P. Lu,[1,42] C. L. Luo,[32] M. X. Luo,[59] P. W. Luo,[43] T. Luo,[9,j] X. L. Luo,[1,42] S. Lusso,[55c] X. R. Lyu,[46] F. C. Ma,[31] H. L. Ma,[1] L. L. Ma,[36] M. M. Ma,[1,46] Q. M. Ma,[1] X. N. Ma,[34] X. X. Ma,[1,46] X. Y. Ma,[1,42] Y. M. Ma,[36] F. E. Maas,[15] M. Maggiora,[55a,55c] S. Maldaner,[26] Q. A. Malik,[54] A. Mangoni,[23b] Y. J. Mao,[35] Z. P. Mao,[1] S. Marcello,[55a,55c] Z. X. Meng,[48] J. G. Messchendorp,[29] G. Mezzadri,[24a] J. Min,[1,42] T. J. Min,[33] R. E. Mitchell,[22] X. H. Mo,[1,42,46] Y. J. Mo,[6] C. Morales Morales,[15] N. Yu. Muchnoi,[10,d] H. Muramatsu,[49] A. Mustafa,[4] S. Nakhoul,[11,g] Y. Nefedov,[27] F. Nerling,[11,g] I. B. Nikolaev,[10,d] Z. Ning,[1,42] S. Nisar,[8,k] S. L. Niu,[1,42] S. L. Olsen,[46] Q. Ouyang,[1,42,46] S. Pacetti,[23b] Y. Pan,[52,42] M. Papenbrock,[56] P. Patteri,[23a] M. Pelizaeus,[4] H. P. Peng,[52,42] K. Peters,[11,g] J. Pettersson,[56] J. L. Ping,[32] R. G. Ping,[1,46] A. Pitka,[4] R. Poling,[49] V. Prasad,[52,42] M. Qi,[33] T. Y. Qi,[2] S. Qian,[1,42] C. F. Qiao,[46] N. Qin,[57] X. S. Qin,[4] Z. H. Qin,[1,42] J. F. Qiu,[1] S. Q. Qu,[34] K. H. Rashid,[54,i] C. F. Redmer,[26] M. Richter,[4] M. Ripka,[26] A. Rivetti,[55c] M. Rolo,[55c] G. Rong,[1,46] Ch. Rosner,[15] M. Rump,[50] A. Sarantsev,[27,e] M. Savrié,[24b] K. Schoenning,[56] W. Shan,[19] X. Y. Shan,[52,42] M. Shao,[52,42] C. P. Shen,[2] P. X. Shen,[34] X. Y. Shen,[1,46] H. Y. Sheng,[1] X. Shi,[1,42] X. D. Shi,[52,42] J. J. Song,[36] Q. Q. Song,[52,42] X. Y. Song,[1] S. Sosio,[55a,55c] C. Sowa,[4] S. Spataro,[55a,55c] F. F. Sui,[36] G. X. Sun,[1] J. F. Sun,[16] L. Sun,[57] S. S. Sun,[1,46] X. H. Sun,[1] Y. J. Sun,[52,42] Y. K. Sun,[52,42] Y. Z. Sun,[1] Z. J. Sun,[1,42] Z. T. Sun,[1] Y. T. Tan,[52,42] C. J. Tang,[39] G. Y. Tang,[1] X. Tang,[1] B. Tsednee,[25] I. Uman,[45d] B. Wang,[1] B. L. Wang,[46] C. W. Wang,[33] D. Y. Wang,[35] H. H. Wang,[36] K. Wang,[1,42] L. L. Wang,[1] L. S. Wang,[1] M. Wang,[36] M. Z. Wang,[35] Meng Wang,[1,46] P. Wang,[1] P. L. Wang,[1] R. M. Wang,[58] W. P. Wang,[52,42] X. Wang,[35] X. F. Wang,[1] Y. Wang,[52,42] Y. F. Wang,[1,42,46] Z. Wang,[1,42] Z. G. Wang,[1,42] Z. Y. Wang,[1] Zongyuan Wang,[1,46] T. Weber,[4] D. H. Wei,[12] P. Weidenkaff,[26] S. P. Wen,[1] U. Wiedner,[4] M. Wolke,[56] L. H. Wu,[1] L. J. Wu,[1,46] Z. Wu,[1,42] L. Xia,[52,42] Y. Xia,[20] Y. J. Xiao,[1,46] Z. J. Xiao,[32] Y. G. Xie,[1,42] Y. H. Xie,[6] X. A. Xiong,[1,46] Q. L. Xiu,[1,42] G. F. Xu,[1] L. Xu,[1] Q. J. Xu,[14] W. Xu,[1,46] X. P. Xu,[40] F. Yan,[53] L. Yan,[55a,55c] W. B. Yan,[52,42] W. C. Yan,[2] Y. H. Yan,[20] H. J. Yang,[37,h] H. X. Yang,[1] L. Yang,[57] R. X. Yang,[52,42] S. L. Yang,[1,46] Y. H. Yang,[33] Y. X. Yang,[12] Yifan Yang,[1,46] Z. Q. Yang,[20] M. Ye,[1,42] M. H. Ye,[7] J. H. Yin,[1] Z. Y. You,[43] B. X. Yu,[1,42,46] C. X. Yu,[34] J. S. Yu,[20] C. Z. Yuan,[1,46] Y. Yuan,[1] A. Yuncu,[45b,a] A. A. Zafar,[54] Y. Zeng,[20] B. X. Zhang,[1] B. Y. Zhang,[1,42] C. C. Zhang,[1] D. H. Zhang,[1] H. H. Zhang,[43] H. Y. Zhang,[1,42] J. Zhang,[1,46] J. L. Zhang,[58,*] J. Q. Zhang,[4] J. W. Zhang,[1,42,46] J. Y. Zhang,[1] J. Z. Zhang,[1,46] K. Zhang,[1,46] L. Zhang,[44] S. F. Zhang,[33] T. J. Zhang,[37,h] X. Y. Zhang,[36] Y. Zhang,[52,42] Y. H. Zhang,[1,42] Y. T. Zhang,[52,42] Yang Zhang,[1] Yao Zhang,[1] Yu Zhang,[46] Z. H. Zhang,[6] Z. P. Zhang,[52] Z. Y. Zhang,[57] G. Zhao,[1] J. W. Zhao,[1,42] J. Y. Zhao,[1,46] J. Z. Zhao,[1,42] Lei Zhao,[52,42] Ling Zhao,[1] M. G. Zhao,[34] Q. Zhao,[1] S. J. Zhao,[60] T. C. Zhao,[1] Y. B. Zhao,[1,42] Z. G. Zhao,[52,42] A. Zhemchugov,[27,b] B. Zheng,[53] J. P. Zheng,[1,42] Y. Zheng,[35] Y. H. Zheng,[46] B. Zhong,[32]

L. Zhou,[1,42] Q. Zhou,[1,46] X. Zhou,[57] X. K. Zhou,[52,42] X. R. Zhou,[52,42] Xiaoyu Zhou,[20] Xu Zhou,[20] A. N. Zhu,[1,46]
J. Zhu,[34] J. Zhu,[43] K. Zhu,[1] K. J. Zhu,[1,42,46] S. H. Zhu,[51] X. L. Zhu,[44] Y. C. Zhu,[52,42] Y. S. Zhu,[1,46] Z. A. Zhu,[1,46]
J. Zhuang,[1,42] B. S. Zou,[1] and J. H. Zou[1]

(BESIII Collaboration)

[1]*Institute of High Energy Physics, Beijing 100049, People's Republic of China*
[2]*Beihang University, Beijing 100191, People's Republic of China*
[3]*Beijing Institute of Petrochemical Technology, Beijing 102617, People's Republic of China*
[4]*Bochum Ruhr-University, D-44780 Bochum, Germany*
[5]*Carnegie Mellon University, Pittsburgh, Pennsylvania 15213, USA*
[6]*Central China Normal University, Wuhan 430079, People's Republic of China*
[7]*China Center of Advanced Science and Technology, Beijing 100190, People's Republic of China*
[8]*COMSATS University Islamabad, Lahore Campus, Defence Road,
Off Raiwind Road, 54000 Lahore, Pakistan*
[9]*Fudan University, Shanghai 200443, People's Republic of China*
[10]*G.I. Budker Institute of Nuclear Physics SB RAS (BINP), Novosibirsk 630090, Russia*
[11]*GSI Helmholtzcentre for Heavy Ion Research GmbH, D-64291 Darmstadt, Germany*
[12]*Guangxi Normal University, Guilin 541004, People's Republic of China*
[13]*Guangxi University, Nanning 530004, People's Republic of China*
[14]*Hangzhou Normal University, Hangzhou 310036, People's Republic of China*
[15]*Helmholtz Institute Mainz, Johann-Joachim-Becher-Weg 45, D-55099 Mainz, Germany*
[16]*Henan Normal University, Xinxiang 453007, People's Republic of China*
[17]*Henan University of Science and Technology, Luoyang 471003, People's Republic of China*
[18]*Huangshan College, Huangshan 245000, People's Republic of China*
[19]*Hunan Normal University, Changsha 410081, People's Republic of China*
[20]*Hunan University, Changsha 410082, People's Republic of China*
[21]*Indian Institute of Technology Madras, Chennai 600036, India*
[22]*Indiana University, Bloomington, Indiana 47405, USA*
[23a]*INFN Laboratori Nazionali di Frascati, I-00044 Frascati, Italy*
[23b]*INFN and University of Perugia, I-06100 Perugia, Italy*
[24a]*INFN Sezione di Ferrara, I-44122 Ferrara, Italy*
[24b]*University of Ferrara, I-44122 Ferrara, Italy*
[25]*Institute of Physics and Technology, Peace Ave. 54B, Ulaanbaatar 13330, Mongolia*
[26]*Johannes Gutenberg University of Mainz, Johann-Joachim-Becher-Weg 45, D-55099 Mainz, Germany*
[27]*Joint Institute for Nuclear Research, Dubna 141980, Moscow region, Russia*
[28]*Justus-Liebig-Universitaet Giessen, II. Physikalisches Institut,
Heinrich-Buff-Ring 16, D-35392 Giessen, Germany*
[29]*KVI-CART, University of Groningen, NL-9747 AA Groningen, Netherlands*
[30]*Lanzhou University, Lanzhou 730000, People's Republic of China*
[31]*Liaoning University, Shenyang 110036, People's Republic of China*
[32]*Nanjing Normal University, Nanjing 210023, People's Republic of China*
[33]*Nanjing University, Nanjing 210093, People's Republic of China*
[34]*Nankai University, Tianjin 300071, People's Republic of China*
[35]*Peking University, Beijing 100871, People's Republic of China*
[36]*Shandong University, Jinan 250100, People's Republic of China*
[37]*Shanghai Jiao Tong University, Shanghai 200240, People's Republic of China*
[38]*Shanxi University, Taiyuan 030006, People's Republic of China*
[39]*Sichuan University, Chengdu 610064, People's Republic of China*
[40]*Soochow University, Suzhou 215006, People's Republic of China*
[41]*Southeast University, Nanjing 211100, People's Republic of China*
[42]*State Key Laboratory of Particle Detection and Electronics,
Beijing 100049, Hefei 230026, People's Republic of China*
[43]*Sun Yat-Sen University, Guangzhou 510275, People's Republic of China*
[44]*Tsinghua University, Beijing 100084, People's Republic of China*
[45a]*Ankara University, 06100 Tandogan, Ankara, Turkey*
[45b]*Istanbul Bilgi University, 34060 Eyup, Istanbul, Turkey*
[45c]*Uludag University, 16059 Bursa, Turkey*
[45d]*Near East University, Nicosia, North Cyprus, Mersin 10, Turkey*

[46]*University of Chinese Academy of Sciences, Beijing 100049, People's Republic of China*
[47]*University of Hawaii, Honolulu, Hawaii 96822, USA*
[48]*University of Jinan, Jinan 250022, People's Republic of China*
[49]*University of Minnesota, Minneapolis, Minnesota 55455, USA*
[50]*University of Muenster, Wilhelm-Klemm-Str. 9, 48149 Muenster, Germany*
[51]*University of Science and Technology Liaoning, Anshan 114051, People's Republic of China*
[52]*University of Science and Technology of China, Hefei 230026, People's Republic of China*
[53]*University of South China, Hengyang 421001, People's Republic of China*
[54]*University of the Punjab, Lahore 54590, Pakistan*
[55a]*University of Turin, I-10125 Turin, Italy*
[55b]*University of Eastern Piedmont, I-15121 Alessandria, Italy*
[55c]*INFN, I-10125 Turin, Italy*
[56]*Uppsala University, Box 516, SE-75120 Uppsala, Sweden*
[57]*Wuhan University, Wuhan 430072, People's Republic of China*
[58]*Xinyang Normal University, Xinyang 464000, People's Republic of China*
[59]*Zhejiang University, Hangzhou 310027, People's Republic of China*
[60]*Zhengzhou University, Zhengzhou 450001, People's Republic of China*

Using 4.48×10^8 $\psi(3686)$ events collected with the BESIII detector, we search for the decays $\chi_{cJ} \to \mu^+\mu^- J/\psi$ through the radiative decays $\psi(3686) \to \gamma\chi_{cJ}$, where $J = 0, 1, 2$. The decays $\chi_{c1,2} \to \mu^+\mu^- J/\psi$ are observed, and the corresponding branching fractions are measured to be $\mathcal{B}(\chi_{c1} \to \mu^+\mu^- J/\psi) = (2.51 \pm 0.18 \pm 0.20) \times 10^{-4}$ and $\mathcal{B}(\chi_{c2} \to \mu^+\mu^- J/\psi) = (2.33 \pm 0.18 \pm 0.29) \times 10^{-4}$, where the first uncertainty is statistical and the second one systematic. No significant $\chi_{c0} \to \mu^+\mu^- J/\psi$ decay is observed, and the upper limit on the branching fraction is determined to be 2.0×10^{-5} at 90% confidence level. Also, we present a study of dimuon invariant mass dependent transition form factor for the decays $\chi_{c1,2} \to \mu^+\mu^- J/\psi$.

*Corresponding author.
zhangjielei@ihep.ac.cn
[a]Also at Bogazici University, 34342 Istanbul, Turkey.
[b]Also at the Moscow Institute of Physics and Technology, Moscow 141700, Russia.
[c]Also at the Functional Electronics Laboratory, Tomsk State University, Tomsk 634050, Russia.
[d]Also at the Novosibirsk State University, Novosibirsk 630090, Russia.
[e]Also at the NRC "Kurchatov Institute", PNPI, Gatchina 188300, Russia.
[f]Also at Istanbul Arel University, 34295 Istanbul, Turkey.
[g]Also at Goethe University Frankfurt, 60323 Frankfurt am Main, Germany.
[h]Also at Key Laboratory for Particle Physics, Astrophysics and Cosmology, Ministry of Education; Shanghai Key Laboratory for Particle Physics and Cosmology; Institute of Nuclear and Particle Physics, Shanghai 200240, People's Republic of China.
[i]Also at Government College Women University, Sialkot-51310, Punjab, Pakistan.
[j]Also at Key Laboratory of Nuclear Physics and Ion-beam Application (MOE) and Institute of Modern Physics, Fudan University, Shanghai 200443, People's Republic of China.
[k]Also at Harvard University, Department of Physics, Cambridge, Massachusetts 02138, USA.

I. INTRODUCTION

The electromagnetic (EM) Dalitz decays $M_1 \to M_2 \ell^+ \ell^-$ (M for meson, $\ell = e$ or μ) provide information on the internal structure of the mesons and the interactions of the mesons with the electromagnetic field [1–4]. Such decays are well studied in light-quark meson sector [5], but very rare in charm sector, let alone in the bottom sector. The q-dependent transition form factor (TFF), where q is the invariant mass of the lepton pair, serves as a sensitive probe to the inner structure of the mesons involved, thus provides crucial tests to the theoretical models developed to describe the nature of the mesons, especially the charmoniumlike states which manifested exotic properties compared with conventional charmonium states. One example is the $X(3872)$; while it is a candidate for the radial excitation of the P-wave charmonium state χ_{c1}, it is also a good candidate of the $D\bar{D}^*$ molecule. Precision measurement of its EM Dalitz decays and comparison with those of χ_{c1} decays and the relevant theoretical models may eventually reveal its nature.

The branching fractions for $\chi_{cJ} \to \mu^+\mu^- J/\psi$ are predicted in Ref. [6] (Throughout this paper, χ_{cJ} refers to χ_{c0}, χ_{c1}, and χ_{c2}), and it is demonstrated that the $\mu^+\mu^-$ decay channels are more suitable for the investigation of $\chi_{cJ} \to \gamma^* J/\psi$ decay vertices than e^+e^- decay channels, which

have been observed at BESIII [7]. Very recently, LHCb reported the observation of $\chi_{c1,2} \to \mu^+\mu^- J/\psi$ [8] and measured the $\chi_{c1,2}$ resonance parameters. At BESIII, since the branching fractions of $\psi(3686) \to \gamma\chi_{cJ}$ can be calculated very precisely, we can measure the absolute branching fractions of $\chi_{cJ} \to \mu^+\mu^- J/\psi$. The branching fractions in theoretical calculations are related to the TFF, so the measurements can provide more constraints on theoretical calculations about TFF correction [6].

In this work, we report the branching fraction measurements of $\chi_{cJ} \to \mu^+\mu^- J/\psi$ by analyzing the cascade decay $\psi(3686) \to \gamma\chi_{cJ}, \chi_{cJ} \to \mu^+\mu^- J/\psi$. Here, the J/ψ is reconstructed in its decay to an e^+e^- or $\mu^+\mu^-$ pair. This analysis uses a data sample of $(4.481 \pm 0.029) \times 10^8 \psi(3686)$ events [9] taken with the BESIII detector [10] operating at BEPCII [11] in 2009 and 2012. In addition, a data sample corresponding to an integrated luminosity of $(44.49 \pm 0.02 \pm 0.44)$ pb^{-1}, taken at $\sqrt{s} = 3.65$ GeV [12], is used to estimate the background from continuum processes.

II. BESIII DETECTOR AND MONTE CARLO SIMULATION

The BESIII detector is a magnetic spectrometer [10] located at the BEPCII [11]. The cylindrical core of the BESIII detector consists of a helium-based multilayer drift chamber (MDC), a plastic scintillator time-of-flight system (TOF), and a CsI(Tl) electromagnetic calorimeter (EMC), which are all enclosed in a superconducting solenoidal magnet providing a 1.0 T magnetic field. The solenoid is supported by an octagonal flux-return yoke with resistive plate counter muon identifier modules interleaved with steel. The acceptance of charged particles and photons is 93% over 4π solid angle. The charged-particle momentum resolution at 1 GeV/c is 0.5%, and the dE/dx resolution is 6% for the electrons from Bhabha scattering. The EMC measures photon energies with a resolution of 2.5% (5%) at 1 GeV in the barrel (end cap) region. The time resolution of the TOF barrel part is 68 ps, while that of the end cap part is 110 ps.

Simulated samples produced with the GEANT4-based [13] Monte Carlo (MC) package which includes the geometric description of the BESIII detector and the detector response, are used to determine the detection efficiency and to estimate the backgrounds. The simulation includes the beam energy spread and initial state radiation (ISR) in the e^+e^- annihilations modelled with the generator KKMC [14]. The signal MC samples are generated using EVTGEN [15] with a q-dependent decay amplitude based on the assumption of a pointlike meson, as described in Refs. [6,16]. The inclusive MC sample consists of the production of the $\psi(3686)$ resonance, the ISR production of the J/ψ, and the continuum processes incorporated in KKMC [14]. The known decay modes are modeled with EVTGEN [15] using branching fractions taken from the Particle Data Group [5], and the remaining unknown decays from the charmonium states

with LUNDCHARM [17]. The final state radiations (FSR) from charged final state particles are incorporated with the PHOTOS package [18].

III. EVENT SELECTION

Candidate events are required to have four charged tracks, with zero net charge, and at least one photon. For each charged track, the distance of the closest approach to the interaction point (IP) is required to be smaller than 1 cm on the radial direction and smaller than 10 cm along the beam axis. The polar angle (θ) of the tracks must be within the fiducial volume of the MDC ($|\cos\theta| < 0.93$).

Photons are reconstructed from isolated showers in the EMC which are at least 20° away from the nearest charged track. The photon energy is required to be at least 25 MeV in the barrel region ($|\cos\theta| < 0.8$) or 50 MeV in the endcap region ($0.86 < |\cos\theta| < 0.92$). In order to suppress electronic noise and energy depositions which are unrelated to the event, the time after the collision at which the photon is recorded in the EMC is required to satisfy $0 \leq t \leq 700$ ns.

According to the study of signal MC, the tracks with momentum larger than 1 GeV/c are assumed to be leptons from J/ψ decay, otherwise they are considered as muons from χ_{cJ} decay. The EMC deposited energy is used to separate electrons and muons from J/ψ, leptons from the J/ψ decay with energy deposited in EMC larger than 1.0 GeV are identified as electrons, less than 0.3 GeV as muons. The J/ψ signal is selected by requiring the invariant mass of the lepton pair to be in the mass region $[3.085, 3.110]$ GeV/c^2. A vertex fit is performed on the four charged tracks to restrict the tracks originated from the IP. In order to reduce backgrounds and improve the mass resolution, a four-constraint (4C) kinematic fit is performed by constraining the total four momentum to that of the initial beams. All the photons are looped with the four tracks in the kinematic fit and only those with a $\chi^2 < 40$ are retained. If there is more than one photon candidate in an event, only the one with the least χ^2 is retained for further analysis.

A study of the $\psi(3686)$ inclusive MC sample shows that, after applying the above selection criteria, the main backgrounds come from the four processes: Cat. I: $\psi(3686) \to \gamma\chi_{cJ}$, $\chi_{cJ} \to \gamma J/\psi$, $J/\psi \to \ell^+\ell^-$; Cat. II: $\psi(3686) \to \pi_1^0\pi_2^0 J/\psi$, $\pi_1^0 \to \gamma\gamma$, $\pi_2^0 \to \gamma\gamma$, $J/\psi \to \ell^+\ell^-$; Cat. III: $\psi(3686) \to \pi_1^0\pi_2^0 J/\psi$, $\pi_1^0 \to \gamma\gamma$, $\pi_2^0 \to \gamma e^+e^-$, $J/\psi \to \ell^+\ell^-$ and Cat. IV: $\psi(3686) \to \eta J/\psi$, $\eta \to \gamma\mu^+\mu^-$, $J/\psi \to \ell^+\ell^-$.

To suppress the backgrounds from Cats. I and II, where one photon is converted into two electrons, a photon-conversion finder [19] is used to reconstruct the photon-conversion vertex. There are no additional requirements in the photon-conversion finder. The distance from the reconstructed conversion vertex to the z axis, R_{xy}, is used to distinguish the photon conversion background from the
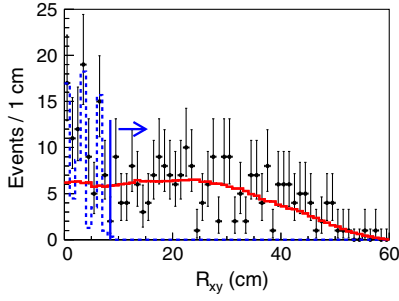
FIG. 1. Distribution of R_{xy} for the decay $\chi_{c1} \to \mu^+\mu^- J/\psi$, where R_{xy} is the distance from the reconstructed conversion vertex to the z axis calculated from the photo-conversion finder [19]. The points with error bars are data, the red histograms are for the signal MC simulations and the blue dotted lines are for the background MC simulations.
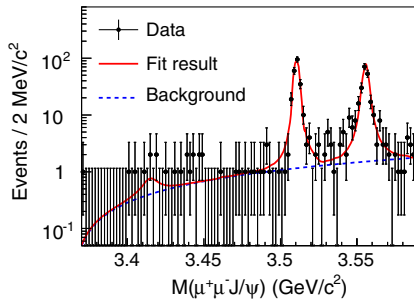

FIG. 2. Distribution of $M(\mu^+\mu^- J/\psi)$ in data (dots with error bars). The solid curve is the overall fit result, the dashed curve is for background contribution.

signal. Figure 1 shows the R_{xy} distribution of the decay $\chi_{c1} \to \mu^+\mu^- J/\psi$ as an example. By studying the MC samples of Cats. I and II, the peaks around $R_{xy} = 3$ and 6 cm match the positions of the beam pipe and the inner wall of MDC [10], respectively. For the background from Cat. III, it enhances around $R_{xy} = 0$ cm. In order to remove all these backgrounds, a requirement $R_{xy} > 8.5$ cm is applied. For the signal events, the reconstructed R_{xy} is almost proportional to the opening angle of the two μ tracks, so if the angle of the two tracks is large, the variable R_{xy} is also large.

To remove the background from Cat. IV, which has the same final state as the signal event, a requirement $M(\gamma\mu^+\mu^-) < 0.535$ or > 0.560 GeV/c^2 is applied, where $M(\gamma\mu^+\mu^-)$ is the invariant mass of $\gamma\mu^+\mu^-$. The requirement removes almost all the Cat. IV background events (it accounts for about 60% of the remaining background, is about 140 events), with an efficiency loss of about 15% for signal events.

After applying all the above criteria for $\psi(3686)$ inclusive MC sample, which does not include the signal processes, only a few events are left, and the overall contribution from $\psi(3686)$ decays in the $M(\mu^+\mu^- J/\psi)$ distribution is found to be smooth. Here $M(\mu^+\mu^- J/\psi) = M(\mu^+\mu^-\ell^+\ell^-) - M(\ell^+\ell^-) + m(J/\psi)$ is used to reduce the resolution effect of the lepton pairs, and $m(J/\psi)$ is the nominal mass of J/ψ [5]. The continuum background is studied by using the data collected at $\sqrt{s} = 3.65$ GeV, and the contribution is found to be negligible.

IV. BRANCHING FRACTION MEASUREMENT

Figure 2 shows the $M(\mu^+\mu^- J/\psi)$ distribution for selected events from data. Clear enhancements at the masses of $\chi_{c1,2}$ are seen, corresponding to the decays $\chi_{c1,2} \to \mu^+\mu^- J/\psi$, while no significant signals for the $\chi_{c0} \to \mu^+\mu^- J/\psi$ decay are found. An unbinned maximum likelihood fit is performed to the $M(\mu^+\mu^- J/\psi)$ distribution to extract the signal yields. We use the MC-determined shapes to describe the χ_{cJ} signals, where the magnitudes are free parameters. The background is described by a linear function with the number of events as free parameter. The fit result is shown in Fig. 2 and the corresponding signal yields are summarized in Table I. The significances for $\chi_{c1,2}$ are larger than 10σ by comparing the likelihood values for the fits with or without $\chi_{c1,2}$ signals and taking the change of the number of degrees-of-freedom into account. Since no significant signal is observed for $\chi_{c0} \to \mu^+\mu^- J/\psi$ decay, we give the upper limit at 90% confidence level (C.L.) using Bayesian method. With the fit function described before, we scan the number of χ_{c0} signal yield to obtain the likelihood distribution, and smear it with systematic uncertainty. The upper limit of the number of χ_{c0} signal yield $N_{\chi_{c0}}^{up}$ at 90% C.L. is obtained via $\int_0^{N_{\chi_{c0}}^{up}} F(x)dx / \int_0^\infty F(x)dx = 0.90$, where $F(x)$ is the probability density function of the likelihood distribution.

The branching fractions $\mathcal{B}(\chi_{cJ} \to \mu^+\mu^- J/\psi)$ are calculated according to

TABLE I. Signal yields, detection efficiency, branching fraction (or upper limit at 90% C.L.) and ratio of the branching fractions for each decay channel. Here the first uncertainty is statistical and the second systematic.

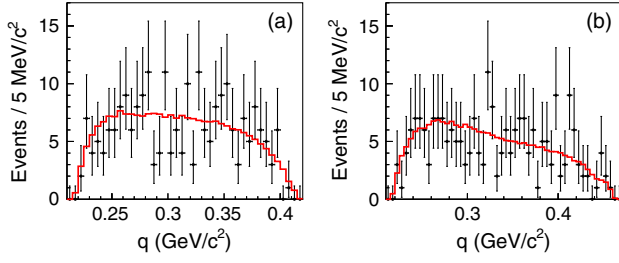| Decay mode	Yields	Efficiency (%)	Branching fraction	$\frac{\mathcal{B}(\chi_{cJ}\to\mu^+\mu^- J/\psi)}{\mathcal{B}(\chi_{cJ}\to e^+e^- J/\psi)}$
$\chi_{c0} \to \mu^+\mu^- J/\psi$	<9.5	9.40	$< 2.0 \times 10^{-5}$	< 0.14
$\chi_{c1} \to \mu^+\mu^- J/\psi$	221.9 ± 15.3	16.94	$(2.51 \pm 0.18 \pm 0.20) \times 10^{-4}$	$(6.73 \pm 0.51 \pm 0.50) \times 10^{-2}$
$\chi_{c2} \to \mu^+\mu^- J/\psi$	218.9 ± 16.1	18.42	$(2.33 \pm 0.18 \pm 0.29) \times 10^{-4}$	$(9.40 \pm 0.79 \pm 1.15) \times 10^{-2}$

FIG. 3. Comparison of q distributions between data and MC simulation. The distributions are not efficiency corrected for the decays $\chi_{c1} \to \mu^+\mu^- J/\psi$ (a) and $\chi_{c2} \to \mu^+\mu^- J/\psi$ (b). The points with error bars are data and the red histograms are for the signal MC simulations. The MC distributions are normalized by the total number of events for data.

$$\mathcal{B}(\chi_{cJ} \to \mu^+\mu^- J/\psi) = \frac{N}{N_{\psi(3686)} \cdot \mathcal{B}_{\mathrm{rad}} \cdot \mathcal{B}_{J/\psi \to l^+l^-} \cdot \epsilon}, \quad (1)$$

where N is the signal yields obtained from the fit, $N_{\psi(3686)}$ is the number of $\psi(3686)$ events [9], ϵ is the average selection efficiency of the decays $J/\psi \to e^+e^-$ and $J/\psi \to \mu^+\mu^-$ determined from the signal MC samples, $\mathcal{B}_{\mathrm{rad}}$ is the branching fraction of the radiative transitions $\psi(3686) \to \gamma\chi_{cJ}$, and $\mathcal{B}_{J/\psi \to \ell^+\ell^-}$ is the sum of branching fractions of $J/\psi \to e^+e^-$ and $J/\psi \to \mu^+\mu^-$. All the branching fractions used are taken from Ref. [5]. The results of $\chi_{cJ} \to \mu^+\mu^- J/\psi$ are listed in Table I.

V. TRANSITION FORM FACTOR MEASUREMENT

Figure 3 shows comparisons of the observed q distributions without efficiency correction in data and MC simulation for the decays $\chi_{c1,2} \to \mu^+\mu^- J/\psi$, where the χ_{c1} and χ_{c2} signals are extracted by requiring a mass within [3.500, 3.520] and [3.545, 3.565] GeV/c^2, respectively; with these criteria the backgrounds are expected to be about 5%. The data are in reasonable agreement with the MC simulation generated by using the pointlike model described in Refs. [6,16].
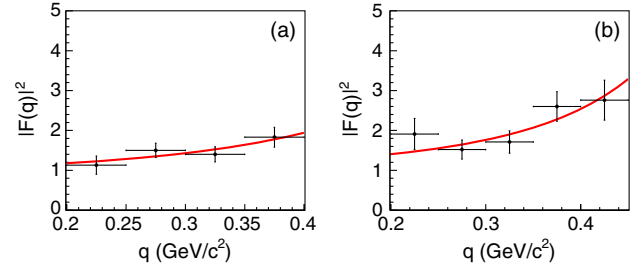

FIG. 4. TFF distributions for the decays $\chi_{c1} \to \mu^+\mu^- J/\psi$ (a) and $\chi_{c2} \to \mu^+\mu^- J/\psi$ (b). The solid curves are the fit results.

To measure the TFF, the q distributions in the decays $\chi_{c1,2} \to \mu^+\mu^- J/\psi$ are divided into 4 and 5 regions, respectively. The bin-by-bin signal yields and corresponding branching fractions are listed in Table II. The quantum electrodynamics (QED) predicted branching fraction results of $\chi_{c1,2} \to \mu^+\mu^- J/\psi$ are obtained from Eq. (2) in Ref. [6], and the uncertainty is from the branching fractions of $\chi_{c1,2} \to \gamma J/\psi$. The TFFs are the ratios of measured branching fractions and QED predicted branching fractions in each bin, which are also listed in Table II. Figure 4 shows the TFF distributions for the decays $\chi_{c1,2} \to \mu^+\mu^- J/\psi$. If we use the parametrization $F(q) = \frac{1}{1 - q^2/\Lambda^2}$ [3] to fit TFF distributions, the fit results are also shown in Fig. 4. The Λ values for the decays $\chi_{c1,2} \to \mu^+\mu^- J/\psi$ are $\Lambda_{\chi_{c1}} = (0.76 \pm 0.18)$ GeV/c^2 and $\Lambda_{\chi_{c2}} = (0.71 \pm 0.10)$ GeV/c^2.

VI. SYSTEMATIC UNCERTAINTY

The systematic uncertainties for the branching fraction measurement arise from the following sources: track reconstruction, photon detection, kinematic fit, J/ψ mass criteria, $M(\gamma\mu^+\mu^-)$ requirement, R_{xy} requirement, fit procedure, angular distribution, number of $\psi(3686)$ events, and the branching fractions of the cascade decays. All uncertainties are discussed in detail below.

The difference between data and MC simulation on the tracking efficiency of high momentum tracks is estimated to be 1% [20] using control sample $\psi(3686) \to \pi^+\pi^- J/\psi$,

TABLE II. Signal yields, measured branching fraction $\mathcal{B}$, QED predicted branching fraction $\mathcal{B}_{\mathrm{QED}}$ [6] and TFF $|F(q)|^2$ for the decays $\chi_{c1,2} \to \mu^+\mu^- J/\psi$ in each bin. Here the first uncertainty is statistical and the second systematic.

Channel	q (GeV/c^2)	Yields	$\mathcal{B}$ (10^{-5})	$\mathcal{B}_{\mathrm{QED}}$ [6] (10^{-5})	$|F(q)|^2$
$\chi_{c1} \to \mu^+\mu^- J/\psi$	$[2m_\mu, 0.25]$	26.9 ± 5.4	$4.32 \pm 0.87 \pm 0.35$	3.81 ± 0.11	$1.13 \pm 0.23 \pm 0.10$
	$[0.25, 0.30]$	74.4 ± 8.9	$8.87 \pm 1.06 \pm 0.71$	5.91 ± 0.17	$1.50 \pm 0.18 \pm 0.13$
	$[0.30, 0.35]$	63.4 ± 8.3	$6.51 \pm 0.85 \pm 0.52$	4.64 ± 0.14	$1.40 \pm 0.19 \pm 0.12$
	$[0.35, 0.40]$	59.5 ± 7.9	$5.17 \pm 0.69 \pm 0.42$	2.83 ± 0.08	$1.83 \pm 0.25 \pm 0.16$
$\chi_{c2} \to \mu^+\mu^- J/\psi$	$[2m_\mu, 0.25]$	29.1 ± 5.9	$4.20 \pm 0.85 \pm 0.52$	2.20 ± 0.06	$1.91 \pm 0.39 \pm 0.24$
	$[0.25, 0.30]$	50.7 ± 7.8	$5.32 \pm 0.82 \pm 0.66$	3.51 ± 0.09	$1.52 \pm 0.24 \pm 0.19$
	$[0.30, 0.35]$	47.4 ± 7.7	$5.02 \pm 0.82 \pm 0.62$	2.93 ± 0.08	$1.71 \pm 0.28 \pm 0.22$
	$[0.35, 0.40]$	56.9 ± 7.9	$5.61 \pm 0.78 \pm 0.70$	2.16 ± 0.06	$2.60 \pm 0.37 \pm 0.33$
	$[0.40, 0.45]$	38.3 ± 6.8	$3.45 \pm 0.62 \pm 0.43$	1.25 ± 0.03	$2.76 \pm 0.50 \pm 0.35$

$J/\psi \rightarrow \ell^+\ell^-$. To study the difference on the low momentum muon tracking efficiency between data and MC simulation, we select a sample of $\psi(3686) \rightarrow \pi^+\pi^- J/\psi$, $J/\psi \rightarrow \mu^+\mu^-\gamma$. The weighted difference between data and MC simulation is about 4% for the low momentum $\mu^+\mu^-$ pair. We also checked $\cos\theta$ dependence of low momentum tracking efficiency using control sample $J/\psi \rightarrow p\bar{p}\pi^+\pi^-$. The π tracking efficiency is $\cos\theta$ dependent, and we use these results to correct the efficiency for $\mu^+\mu^-$ pair, while the weighted difference between data and MC simulation is also about 4%. Totally, a 6% systematic uncertainty on tracking efficiency is attributed to all channels. The uncertainty on the photon detection efficiency is derived from a control sample of $J/\psi \rightarrow \rho^0\pi^0$ and is 1.0% per photon [21].

In the 4C kinematic fit, the helix parameters of charged tracks are corrected to reduce the discrepancy between data and MC simulation as described in Ref. [22]. The correction factors are obtained by studying a control sample of $\psi(3686) \rightarrow \pi^+\pi^- J/\psi$, $J/\psi \rightarrow \ell^+\ell^-$. To determine the systematic uncertainty from this source, we determine the efficiencies from the MC samples without the helix correction; the resulting differences with respect to the nominal values are taken as systematic uncertainties.

The uncertainty associated with the J/ψ mass requirement is 1.0%, which is determined by studying a control sample of $\psi(3686) \rightarrow \eta J/\psi$, $\eta \rightarrow \gamma\gamma$ (where one γ undergoes conversion to an e^+e^- pair) or $\eta \rightarrow \gamma e^+e^-$ decays. The systematic uncertainty related to the $M(\gamma\mu^+\mu^-)$ requirement is studied by removing the requirement and then repeat the analysis to get the result. The difference from the nominal result is taken as systematic uncertainty from this source. Likewise to estimate the systematic uncertainty from R_{xy} requirement, we also remove the requirement to get the result and the difference is taken as systematic uncertainty. Due to the absence of χ_{c0} signal, the uncertainties for χ_{c0} channel on $M(\gamma\mu^+\mu^-)$ requirement and R_{xy} requirement are taken from the larger one in the χ_{c1} and χ_{c2} channels.

The sources of uncertainty in the fit procedure include the fit range, the signal shape, and the background shape. The uncertainty related to the fit range is obtained by varying the limits of the fit range by ± 5 MeV/c^2. The largest difference in the signal yields with respect to the nominal values is taken as systematic uncertainty. In the nominal fit, the signal shapes are described with the MC simulated signal shapes. An alternative fit is performed with the signal MC simulated shapes convolved with a Gaussian function. The resulting change in the signal yields is taken as systematic uncertainty. The uncertainty associated with the background shape is estimated by an alternative fit replacing the first order polynomial function with a second order polynomial function. The change in the signal yields is taken as systematic uncertainty. About the uncertainty from fit procedure for χ_{c0} channel, we try to use different combinations of fit range, signal shape, and

TABLE III. Summary of systematic uncertainties (in %). $\cdots$ means that the results are not applicable.

	$\chi_{cJ} \rightarrow \mu^+\mu^- J/\psi$		
	χ_{c0}	χ_{c1}	χ_{c2}
Tracking	6.0	6.0	6.0
Photon	1.0	1.0	1.0
Kinematic fit	2.6	2.5	2.5
J/ψ mass window	1.0	1.0	1.0
$M(\gamma\mu^+\mu^-)$ requirement	6.0	1.8	6.0
R_{xy} requirement	7.6	2.7	7.6
Fit range	$\cdots$	0.5	2.1
Signal shape	$\cdots$	0.1	0.4
Background shape	$\cdots$	0.2	2.3
Angular distribution	2.7	1.1	0.1
Number of $\psi(3686)$	0.7	0.7	0.7
Branching fractions	2.1	2.5	2.1
Sum	12.3	8.0	12.4

background shape to get the upper limits, and choose the largest one as nominal upper limit.

The helicity angle distribution $1 + \alpha \cdot \cos^2\theta$ of the $\mu^+\mu^-$ pair in χ_{cJ} rest frame may affect the detection efficiency, where α is angular distribution parameter. We fix the angular distribution of $\mu^+\mu^-$ pair in $\chi_{c1,2} \rightarrow \mu^+\mu^- J/\psi$ at the measurements from processes $\chi_{c1,2} \rightarrow e^+e^- J/\psi$ [7], $\alpha_{\chi_{c1}} = 0.0 \pm 0.2$ and $\alpha_{\chi_{c2}} = 0.5 \pm 0.2$, and vary 1σ to get the systematic uncertainty. For the decay $\chi_{c0} \rightarrow \mu^+\mu^- J/\psi$, the angular distribution of $\mu^+\mu^-$ pair is set to be flat, and varied to $1 \pm \cos^2\theta$ to get the systematic uncertainty.

The number of $\psi(3686)$ events is measured with an uncertainty of 0.7% by using the inclusive hadronic events [9]. The uncertainties of the branching fractions in the cascade decays are taken from Ref. [5].

Table III summarizes all individual systematic uncertainties, and the overall uncertainties are the quadrature sums of the individual ones, assuming they are independent. The overall uncertainties are also taken as the systematic uncertainties of the branching fraction measurements for the decays $\chi_{c1,2} \rightarrow \mu^+\mu^- J/\psi$ in each bin in Table II.

VII. RESULTS AND DISCUSSION

In summary, we observe the decays $\chi_{c1,2} \rightarrow \mu^+\mu^- J/\psi$ through the radiative transitions $\psi(3686) \rightarrow \gamma\chi_{cJ}$. The corresponding branching fractions are measured for the first time to be $\mathcal{B}(\chi_{c1} \rightarrow \mu^+\mu^- J/\psi) = (2.51 \pm 0.18 \pm 0.20) \times 10^{-4}$ and $\mathcal{B}(\chi_{c2} \rightarrow \mu^+\mu^- J/\psi) = (2.33 \pm 0.18 \pm 0.29) \times 10^{-4}$, where the first uncertainty is statistical and the second systematic. We do not observe significant $\chi_{c0} \rightarrow \mu^+\mu^- J/\psi$ events, and an upper limit at 90% C.L. on the branching fraction is set to be $\mathcal{B}(\chi_{c0} \rightarrow \mu^+\mu^- J/\psi) < 2.0 \times 10^{-5}$. The ratios of branching fractions $\frac{\mathcal{B}(\chi_{cJ} \rightarrow \mu^+\mu^- J/\psi)}{\mathcal{B}(\chi_{cJ} \rightarrow e^+e^- J/\psi)}$ are also

obtained by incorporating the BESIII measurements of the branching fractions $\mathcal{B}(\chi_{cJ} \to e^+e^- J/\psi)$ in Ref. [7], as listed in Table I. The common systematic uncertainties related to efficiency and branching fractions cancel in the calculation. From the measured TFF distributions, the $|F(q)|^2$ values deviate from one significantly. This indicates that the TFF should be considered in the branching fraction calculation. If we use the parametrization $F(q) = \frac{1}{1-q^2/\Lambda^2}$ to parametrize TFF with $\Lambda = m_\rho = 0.77$ GeV/c^2, the calculated branching fractions [6] for $\chi_{cJ} \to \mu^+\mu^- J/\psi$ agree well with the measured results.

[1] R. H. Dalitz, Proc. Phys. Soc. London Sect. A **64**, 667 (1951).

[2] L. G. Landsberg, Phys. Rep. **128**, 301 (1985).

[3] J. Fu, H. B. Li, X. S. Qin, and M. Z. Yang, Mod. Phys. Lett. A **27**, 1250223 (2012).

[4] H. B. Li and T. Luo, Phys. Lett. B **686**, 249 (2010).

[5] M. Tanabashi *et al.* (Particle Data Group), Phys. Rev. D **98**, 030001 (2018).

[6] A. V. Luchinsky, Mod. Phys. Lett. A **33**, 1850001 (2018).

[7] M. Ablikim *et al.* (BESIII Collaboration), Phys. Rev. Lett. **118**, 221802 (2017).

[8] R. Aaij *et al.* (LHCb Collaboration), Phys. Rev. Lett. **119**, 221801 (2017).

[9] M. Ablikim *et al.* (BESIII Collaboration), Chin. Phys. C **42**, 023001 (2018).

[10] M. Ablikim *et al.* (BESIII Collaboration), Nucl. Instrum. Methods Phys. Res., Sect. A **614**, 345 (2010).

[11] C. H. Yu *et al.*, *Proceedings of IPAC2016, Busan, Korea* (JACoW, Geneva, Switzerland, 2016).

[12] M. Ablikim (BESIII Collaboration), Chin. Phys. C **37**, 123001 (2013).

[13] S. Agostinelli *et al.* (GEANT4 Collaboration), Nucl. Instrum. Methods Phys. Res., Sect. A **506**, 250 (2003).

[14] S. Jadach, B. F. L. Ward, and Z. Was, Phys. Rev. D **63**, 113009 (2001); Comput. Phys. Commun. **130**, 260 (2000).

[15] D. J. Lange, Nucl. Instrum. Methods Phys. Res., Sect. A **462**, 152 (2001); R. G. Ping, Chin. Phys. C **32**, 599 (2008).

[16] A. Faessler, C. Fuchs, and M. I. Krivoruchenko, Phys. Rev. C **61**, 035206 (2000).

[17] J. C. Chen, G. S. Huang, X. R. Qi, D. H. Zhang, and Y. S. Zhu, Phys. Rev. D **62**, 034003 (2000); R. L. Yang, R. G. Ping, and H. Chen, Chin. Phys. Lett. **31**, 061301 (2014).

[18] E. Richter-Was, Phys. Lett. B **303**, 163 (1993).

[19] Z. R. Xu and K. L. He, Chin. Phys. C **36**, 742 (2012).

[20] M. Ablikim *et al.* (BESIII Collaboration), Phys. Rev. D **93**, 011102 (2016).

[21] M. Ablikim *et al.* (BESIII Collaboration), Phys. Rev. Lett. **116**, 251802 (2016).

[22] M. Ablikim *et al.* (BESIII Collaboration), Phys. Rev. D **87**, 012002 (2013).